2017 WSGC Elijah High-Altitude Balloon Payload

Nicholas M. Hennigan[1], Stuart Oliphant[3], Tyler T. Rasmussen[2], Frederick M. Rosenberger[1], and Blaine T. Vollmer[1]
Milwaukee School of Engineering[1], University of Wisconsin-Fox Valley[2], University of Wisconsin-Platteville[3]

Abstract

The 2017 WSGC Elijah High-Altitude Balloon Payload Fellowship focused on three different topics for high altitude research: Modular Payload Design, Balloon Dynamics, and Energy Harvesting. A modular payload system was created using advanced manufacturing methods, which improved assembly and field operation. Minor structural fracturing was observed upon recovery. All instrumentation recovered were functioning. Vertical flight dynamics of a high-altitude balloon were studied to create a model that was compared against experimental data. Predictions did not accurately replicate GPS altitude data, possibly due to incorrect internal-balloon pressure readings and underlying assumptions. Habitability of high-altitude environments were explored by monitoring insect analog in pressurized environment. A slow pressure leak induced insects into a comatose state. Radiation was detected visually with camera. Investigated energy generation from balloon kinematics. Flight data not obtained but flight simulation data produced average voltage = 0.0039 V and total energy = 245.13 J.

1. Overview

The Elijah Balloon fellowship is a research program established by the consortium with the intention of enabling undergraduates in STEM fields to gain research experience via a high-altitude balloon platform. This year's team explored different facets of long-term high-altitude ballooning, including, modular payload design concepts, balloon flight dynamics, energy harvesting, and radiation shielding. This research not only benefits the students, but also the scientific body by bringing new minds into academic research. With companies like Google and World View showing interest in prolonged high-altitude flights, there is reason to believe this research will benefit many in the coming years.

2. Payload Construction

2.1 Introduction The objective of the payload construction project was to develop a modular payload design that could support removable shelves, protect scientific experiments from harmful conditions, incorporate an audible recovery beacon, and provide onboard video.

2.2 Method System design was conceptualized and developed in Onshape, an open source 3D-modeling online software. The utilization of a collaborative CAD software enabled the team to determine flaws and conflicts in the model before anything was manufactured.

The use of 3D-printers increased design efficiency. Small-scale testing found that 3D-printers were unable to print the main support structure in a single print. As a result, modularity was increased by designing individual shelf support sections that joined together via interlocking conflict joints. The joints were fine-tuned to provide a secure yet separable fit. These small-scale tests greatly reduced the amount of time and material required for prototyping, when compared to more traditional methods.

During flight, scientific payloads experience drastic changes in temperature that can result in deformations of certain materials; most plastics are exceptionally vulnerable to this phenomenon

Acknowledgments: Wisconsin Space Grant Consortium and Advisor Dr. William Farrow

called thermal expansion. MSOE supplied the two types of 3D-printer filament: acrylonitrile butadiene styrene (ABS) and polylactic acid (PLA). ABS is an extremely versatile plastic whose properties can be easily altered by synthesizing it with varying amounts of its three monomers: acrylonitrile, butadiene, and styrene (Chang) (Kulich 2001, 2003). As a terpolymer—a copolymer possessing three monomers—ABS inherits a wide variety of properties from its substituents, such as, toughness at reduced temperatures from polybutadiene, strength from the intermolecular hydrogen bonding with the nitrile groups, and homogeneity from the styrene. All parts were printed with ABS, as opposed to PLA, for its higher resistance to thermal changes within the temperature range experienced during flight. ABS is also relatively forgiving in the 3D-printing process, a quality that was desired since prior to this project none of the team members had experience with 3D-printing.

Laser cutting was used in the production of the shelves. The required 2D-models were generated in Onshape and opened in AutoCAD for laser cutting. In the past, payload shelves were often made of birch plywood. Tests were conducted on shelves laser cut from birch plywood and compared to shelfs cut from foam-core. Tests showed that although foam-core was weaker than the birch plywood, it met stress/strain requirements while being $1/7^{th}$ the mass.

To protect the scientific experiments, the payload design addressed three major threats: convective heat loss, thermal radiation, and electrical water damage. Electronic circuitry can be adversely affected by convective heat loss as a cold body, the air, absorbs heat energy from the system. To reduce convective heat loss, the payload was surrounded by extruded polystyrene. This material provides ample insulation while possessing a low enough strength to comply with FAA restrictions. To produce the surrounding sleeve, foam was cut with a hot-wire into eight cylinders, six of which had their centers removed via similar process producing a one-inch thick shell wall. These six rings and one solid cylinder were then glued together to produce the sleeve. To protect against thermal radiation, the sleeve and the remaining cylinder were wrapped in metallized BoPET (Biaxially-oriented polyethylene terephthalate) film, which acts as a reflector of electromagnetic waves. To prevent water damage to the electronics from condensation or a water landing, a hydrophobic coating was applied directly to the circuitry, in the form of a silicone conformal coating.

In an attempt to expedite the recovery of the payload should its landing sight not be visible, a high-pitched audible beacon system was designed to engage upon descent. For this, two piezo electric speakers were fastened to the exterior of the payload and programmed to emit alternating audio signals. It is traditional to capture video of balloon flights as a form of documentation. Two YI action cameras were mounted to the top of the payload, one facing up towards the balloon and the other facing down capturing video of the earth and the payload. To provide both cameras with enough back-up power for the entirety of the flight, a 10,000 mAh power bank was integrated into the camera mount.

2.3 Results Upon impact with the ground, the mounting prongs of the bottom section of the shelving system buckled. Although an unexpected failure, it may have resulted in the absorption of the energy from impact, in theory, preventing damage to the scientific experiments. The lower vertical shelf system was also damaged from the impact. Material was removed from this section to save weight, however, this compromised the integrity of the foam board, allowing it to buckle. All other shelves in the payload remained intact, suffering no damage of mention.

Temperature measurements inside the payload remained steady throughout much of the flight, however, there is some doubt as to whether this was a result of the insulation or due to the temperature sensor being mounted near the batteries. For reasons unknown, the audible recovery beacon prematurely engaged during flight and then disengaged shortly after burst. Both cameras successfully captured video of the ascent and descent, however, each faced their own shortcomings. The downward facing camera was broken from its mount shortly after burst and returned with the payload via the safety line that was attached to it. Whereas, the upward facing camera stopped recording shortly before impact with the ground, believably due to the impact causing data corruption.

2.4 Conclusion There are many ways in which future teams could continue the research of the payload assembly. It would be possible for a team to produce their own blend of ABS, allowing them to emphasize specific properties desirable for high-altitude balloon flights. Further research could go into the development of an error-proofed code that would allow the audible beacons to function properly. Temperature probes could be placed throughout the interior in attempt to determine how much heat is a result of battery usage. Additionally, a mounting system could be developed to prevent lines from wrapping around the mounting bracket for the cameras.

3. Balloon Dynamic Modeling

The objective of this experiment is to create a mathematical model that describes the dynamics of a high-altitude balloon ascent and verify model accuracy with experimental data.

3.1 Introduction High-altitude balloons use the properties of buoyancy to carry payloads into the upper stratosphere. The balloon's behavior is dependent on many complex and interrelated factors involving buoyancy, gravity, volume, pressure, temperature, drag and hyperelasticity. By understanding how these factors behave mathematically, it is possible to create an algorithmic simulation of the balloon's behavior.

According to a journal written in 1909 by A. Osborne titled "Elasticity of Rubber Balloons and Hollow Viscera", household balloons and similar thin walled elastic membranes, experience an initial spike in internal pressure. If inflated again, the internal pressure spike is always less than the first attempt. Osborne coined this phenomenon "initial rigidity" (pg. 489, para. 2). The book the "Theory of Elasticity" (L.D Landau & E.M Lifshitz, 1970) explains, with some assumptions, A. Osborne's phenomena by looking at the strain properties of rubber for small deformations. Later research yielded promise in theory of hyperelasticity. Most specifically, the Gent and Mooney-Rivlin model (Nomesh & Venkateswara, 2016). Further research is needed before applying hyper-elastic strain properties to the current model. Understanding how rubber behaves and the strain relations between varying sizes of elastic is needed to begin the process of numerically validating the model.

3.2 Method A mathematical model was created to simulate the vertical ascent of a 1600 gram high-altitude balloon. As shown in Figure 1, the model utilizes numerical integration to determine the ascent rate and altitude of the balloon at incremental time steps. Initially the model contained many assumptions, which were progressively eliminated to increase accuracy. The initial conditions used to generate the progressive models and a summary of the parameters accounted for are listed below.

Progressive Model Initial Conditions:

- Initial radius
- Final radius
- Drag coefficient
- Initial altitude
- Maximum altitude

Summary of Parameters Accounted For:

- Changing Atmosphere
- Ideal Gas Law Expansion
- Changing Gravity
- Balloon Elastic Pressure
- Non-Spherical Frontal Are

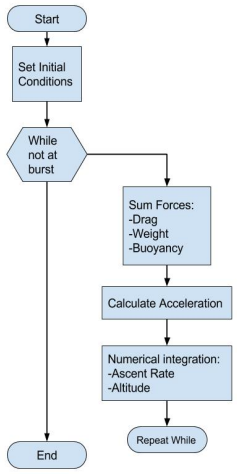

Figure 1: Model Flowchart

As shown in Figure 2, each new model is built upon the previous to show the development and increased accuracy of the simulation as assumptions are eliminated.

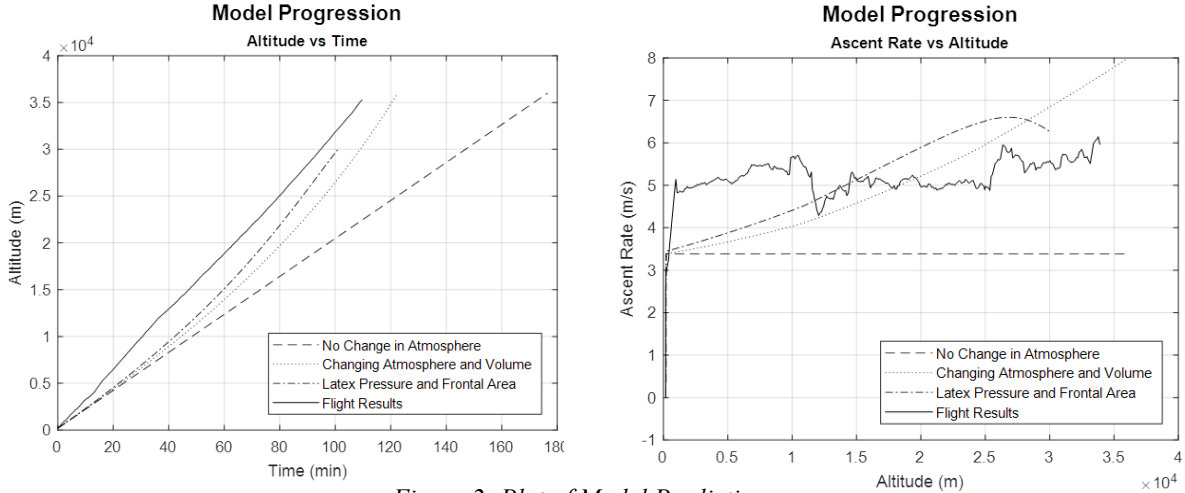

Figure 2: Plot of Model Predictions

The final model is not completely void of assumptions, and a brief list of the parameters that were not accounted for are listed below

Parameters Unaccounted For:

- Changing Drag Coefficients
- Heat Transfer
- Hyperelasticity
- Latex Properties with Temperature

Data was collected during the balloon flight in an effort to calibrate the model and determine its accuracy. Pressure and temperature was recorded inside the throat of the balloon as well as outside the main payload to generate balloon data curves to compare and update model predictions. Shortly before launch the thermocouple used to measure the temperature of the outside air suffered an equipment malfunction and failed to record data for the duration of the flight. To investigate the balloon expansion as altitude increased, cameras were mounted on top of the payload to record the frontal area of the balloon during the ascent. Altitude data from the GPS module was collected to create altitude and ascent rate plots for model comparison.

3.3 Results: Preflight predictions were made by performing small scale experiments to generate pressure and geometric data. The experiments were conducted on both a 50-gram and a 200-gram latex balloon. The results of the experiments were scaled using an equivalent stress assumption to represent the 1600-gram latex balloon. Post-flight, an updated version of the model was created by replacing the data from the small scale experiments with data collected during the ascent. Results of the model predictions are compared to the flight data collected by the GPS in Figure 3.

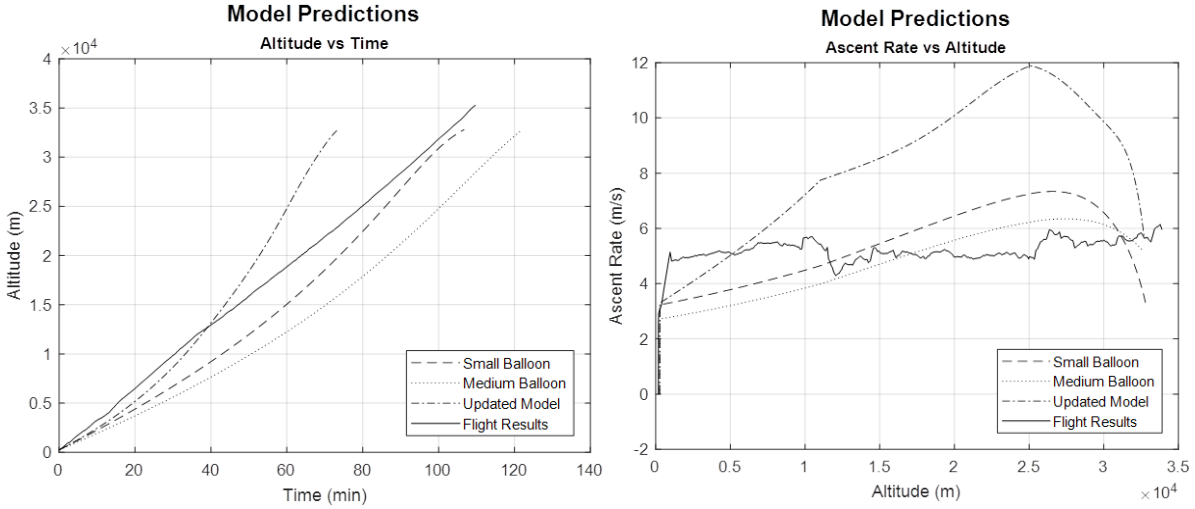

Figure 3: Model Predictions

The most accurate model prediction was the small balloon simulation largely due to its pressure curve. The updated model prediction, which uses data recorded from the flight, had a much higher speed because the more accurate temperature data led to an increase buoyant force. All of the model predictions resulted in a balloon burst before reaching the altitude found during flight.

3.4 Conclusion The model predictions did not accurately replicate the GPS altitude data collected during flight. The main source of error is believed to be incorrect pressure readings from inside the balloon, which resulted from the pressure being measured at the base of the non-spherical balloon.

Recommendations for future work on developing a more accurate model include the investigation of changing drag coefficients, balloon heat transfer, and hyperelastic pressure calculations. The drag coefficients change with the size of the balloon, air density, and air speed. Small scale models should be constructed and analyzed in a wind tunnel or advanced CFD could be performed. The temperature inside the balloon was measured during flight but was not modeled in the small and medium predictions. The effect of not modeling the heat transfer results in less buoyancy due to

ideal gas expansion because the temperature is assumed to be that of the outside environment. The modeling of the balloon pressure was greatly simplified by using experimental elastic pressure curves to calculate volume. More useful detail may be obtained with less assumptions by using hyperelasticity calculations to determine the elastic pressure provided by the balloon. By accounting for these parameters in one comprehensive model, it is possible to accurately simulate and predict the vertical ascent of a high-altitude balloon.

More project details, along with the full MATLAB code, are available at www.Balloon-Dynamic-Modeling.weebly.com

4. Energy Harvesting

The objective of the energy harvesting project was to investigate the natural kinematics of the high-altitude payload and transform its motion into usable electric energy to power on board electronic devices. This was done in both the throat payload as well as the main payload.

4.1 Introduction Energy harvesting is the act of capturing energy from an external source of generation. The balloon's kinematics is caused by wind turbulence during flight. During the balloons assent to 115,000 ft, it experiences drastic changes in wind speed from 20 mph to 60 mph, which the on-board energy harvester uses to generate electrical output. (Biba, 2009) Harvesting energy from this process has many applications including potential to power remote electronic devices in weather balloons. The electronics used in the main payload required a constant 5 V of power, and the throat payload required a constant 3.3 V of power.

4.2 Methods Mass, physical size, reliability, and electrical power output were the design constraints. Devices considered were: piezoelectric vibration sensor and a magnet-coil device. A piezoelectric vibration sensor works by activating silicon quartz crystals within the device through bending of the sensor. During testing, the amount of acceleration required to activate the sensor was too high for project applications and disregarded.

Magnet-coil device testing was found to be very promising from early stages. Initial testing consisted of wrapping magnet wire around a PVC tube, placing a magnet inside of the tube and oscillating the magnet while reading voltage on an oscilloscope. This simple contraption gave minimal voltage values in the range of 200 - 400 mV. The second test was placing the device in a larger PVC tube tethered to a ceiling and replicating the payload's movement based upon previous year's flight footage. The magnet-coil device, seen in Figure 5, was derived from a shake flashlight as the coils and magnet in the flashlight were perfectly suited for this experiment. Later testing incorporated springs at each of the ends of the plastic tube to increase voltage output by increasing the number of oscillations of the magnet with the same force applied, but testing concluded it had a damping effect to the main tube. The voltage generated from this model was significantly more than the initial test (0.8 - 6.4 V).

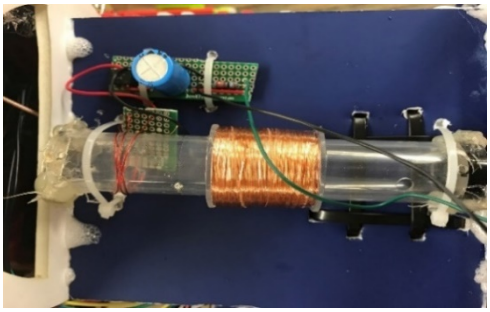

Figure 5: Magnet-Coil Device

After testing and building the magnet-coil device for the payload, a quarter scale model was made for the throat of the balloon. Eq (1) calculates electrical resistivity through a wire of a given cross sectional area, A. Eq (1) was used to find the required wire length needed to mimic performance of the pre-wrapped spool from the flashlight. This equation uses the resistivity of the material, cross sectional area, and resistance of the material to compute the length of wire.

$$R=\frac{\rho L}{A} \qquad (1)$$

25 m of annealed copper wire was wrapped for the quarter scale device in the throat payload. Tests of the quarter scale model produced 400 mV at its maximum output, which would not overcome the 600 mV voltage drop brought on by the four-bridge rectifier in the circuit. To measure the energy produced by the harvesting unit, a circuit was built using a 225 precision resistor, a 2200 F 15 V capacitor, and a four-bridge rectifier to convert the alternating current into direct current. Two leads are attached to the resistor, one for reading the voltage by the Arduino 101, and one for ground. The same circuit was built for the quarter scale model using a smaller value resistor and capacitor.

4.3 Results The magnet-coil energy harvesting unit was not connected correctly before flight, so no true flight data collected for the main payload. The data recorded in the throat payload amounted to zero volts accumulated, but did prove the ability for data to be transmitted from the throat to the main payload. Post-launch tests were done to simulate the flight according to video captured during flight. Figure 6 simulates the voltage generation of the first 30-minutes after balloon launch. Voltage readings were taken twice per second by the Arduino controller. The X-axis title "Data Points" refers to the total amount of readings taken during the test. Voltage generated was lower than expected. Using the recorded voltage values from the simulated flight and known resistance value, Eq (2) was used to compute electrical power output. Total electrical energy, Eq (3), is found by multiplying total accumulated power by the total amount of time.

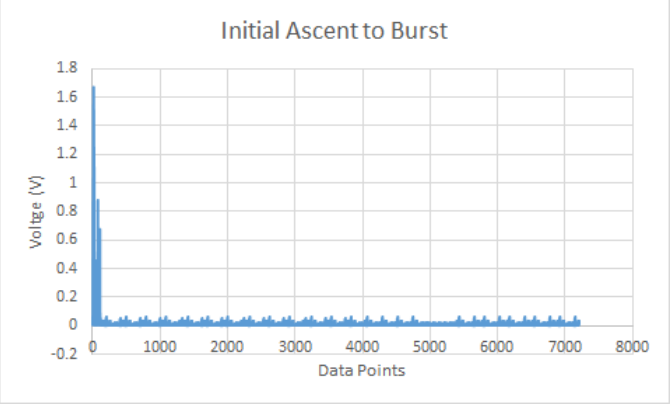

Figure 6: Magnet-Coil Voltage Output per Sample Reading of Arduino Controller

$$P=V^2R \qquad (2)$$

$$E=P\times t \qquad (3)$$

The average voltage produced in the 30 minute test was 0.0039 V and the total energy produced was 245.13 J. To simulate the descent of the payload, a 29-second test was performed with the average voltage being 1.48 V. The difference in energy output between the ascent and descent tests was .89 J : 2.18 J, which promotes the idea of using the energy harvesting unit on the descent.

4.4 Conclusion The flight simulation data showed the ascent of the balloon does not provide enough energy to power any electronic devices within the payload. Due to a preflight improper connection, there cannot be a true conclusion drawn, but the supplementary testing leans towards this conclusion. The energy harvesting unit used does however have the potential to power a device on the descent. The recordings transmitted from the throat payload conclude that the payload did not experience enough accelerations on its ascent to power a device in that payload. To avoid electronic failures and data loss, future flights should incorporate checking the payload electronics system by turning the electronics on and then taking out the SD cards to check if data is being properly recorded.

5. Bug Habitat

The objective was to maintain optimal human habitable conditions as stated: pressure to be above 69.64 kPa, temperature to remain within 65°C to 80 °C, and radiation detection to not go over 350 counts per minute (cpm).

5.1 Introduction The variables selected for experimentation show that a quantity of air must be constrained to a volume to maintain the pressure requirement, this is best done with a container that is not permeable with respect to air.

The type of radiation selected to be shielded was cosmic rays. The flight path of this radiation never enters the magnetosphere. The magnetosphere is located in earth's atmosphere where its magnetic field traps charged particles; this location also shields life on earth from harmful radiation. To shield against cosmic rays and the showers they cause, hydrogen atoms were chosen due to their molecular weight being similar to charged radiation particles. This similarity allows hydrogen atoms to absorb the radiation particles momentum. High-Density Polyethylene (HDPE) was selected for its high hydrogen content.

5.2 Method The pressure vessel needed to hold a pressure sensor, temperature sensor, a living specimen, and enough air that it could breathe for the duration of the experiment. To operate internal sensors, wires were threaded through the side of a plastic container. To accommodate the full experiment, the following components had to be included: a micro controller, battery, data logger, Geiger counter, camera to capture specimen behavior during flight, and light source to illuminate specimen for photography. For simplification, micro controller, data logger and battery were housed outside of pressure container and not duplicated for experimental and control sensors. From this research, a 4 oz. HDPE bottle was selected. HDPE is opaque necessitating the bottle to also hold the camera.

Shown in figure 7, the wiring through the side of the container was done by melting the plastic around the pins creating neat square holes. HDPE has a melting point below solder's melting point. This caused the initial tight-fitting holes to be melted wider that needed. To secure the pins and seal the holes, hot glue was used. the resulting set up encountered issues and a new 4 oz. jar was developed.

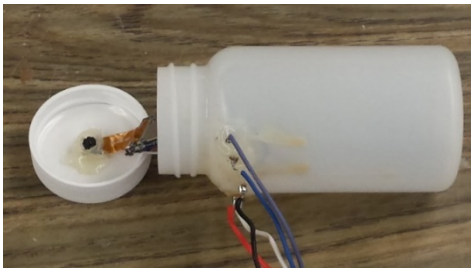

Figure 7 Initial pressure chamber with components

A new jar seen in Figure 8, was selected and made of polyethylene terephthalate. The materials melting point was above soldering temperature, but lower than the max temperature of a soldering iron. Furthermore, sealant was applied to the inside surface the holes instead of the exterior. The focus distance for the camera was increased creating better photos. While neither container passed testing for maintaining atmospheric pressure while within a vacuum, the second iteration showed a slower leak.

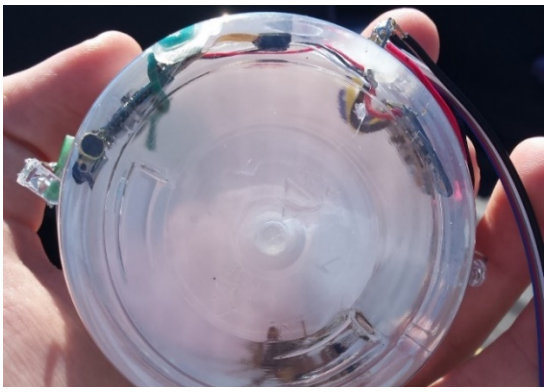

Figure 8 Second iteration of pressure chamber set to fly, being sealed while housing a cricket

To further reduce weight, the bottle was not shielded. To test radiation levels, one Geiger counter was shielded by HDPE sheeting. The one-inch sheeting was cut into 2 inch squares to construct a 2-inch cube that enclosed the Geiger counter. The groove that the Geiger occupied was milled and then trimmed to fit with a chisel. To glue the HDPE squares together silicon sealant was utilized.

The Geiger selected was not built around a photocell. With no Geiger-Muller tube the weight and cost was reduced; furthermore, there was no high voltage circuit. Considerable thought was placed in acquiring an instrument to determine the absorbed radiation levels (e.g. dosimeters). Professional servicing for dosimeter was dropped due to time constraints of the launch deadline.

As a failsafe for the test flight, living specimens were placed inside as a pass-fail result. With a living specimen, onboard lighting and photography was setup to record their experience. For a specimen, an active behavior was wanted; alongside, easy to acquire and low cost. from these requirements, it was determined to fly crickets.

5.3 Results The Failsafe of the pass-fail for the crickets was needed with the loss of data. Health of the crickets, along with video data of their activity to slightly before the bursting of the balloon was analyzed. Other temperature sensors did record the temperature within the payload chamber albeit at a different location near a heat source, battery pack. The results of this can be seen in figure 9 temperature graph. With the knowledge of the chamber having a leak, and the cold temperature experienced, it is surprising that the crickets lived. Their behavior as they slowly enter a comatose state was nicely caught on video. This comatose state is what kept them alive with the lower metabolic rate. Other supporting research indicates that crickets can recover after experiencing zero degree temperatures for long periods. Within the video of the crickets, radiation was detected on camera. See figure 10.

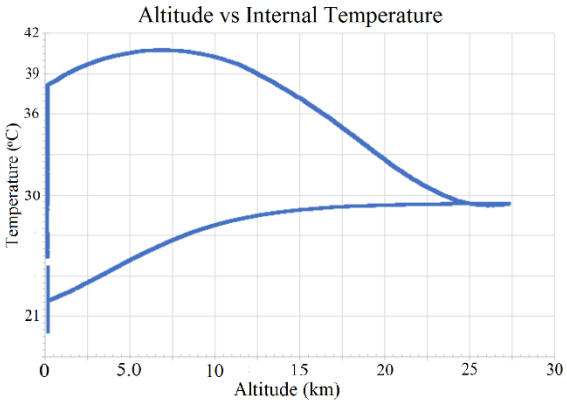

Figure 9 Graph of internal temperature as the payload ascended

5.4 Conclusion Avoid designing a "ship in the bottle" contraption if possible. The initial jar design was not the best choice for its size and number of sensors placed inside. When mounting sensors to lid, design the element to bear torque loads. Write launch/recovery protocols and follow them. When operating an experiment with living specimens, observe them for a time after testing is completed. The length of time that it took the crickets to recovery from the trip to 115,000 ft was not observed. Crickets are a hardy insect that can take extreme environment conditions. It would have been convenient to know the oxygen consumption rate of the crickets, to further understand the results of their varying activity levels during flight.

Acknowledgements

Dr. William Farrow[1]
Roger Haijney[1]
Vivian Mickelson[1]
Dr. Nathan Patterson[1]
Dr. Konstantin Sobolev[2]
Justin Sommers[1]
Dr. Michael Swedish[1]
Richard Phillips[1]
Dr. Prabhakar Venkateswaran[1]
Milwaukee School of Engineering[1], University of Wisconsin-Milwaukee[2]

Disclaimer

This material is based upon work supported by NASA under Award No. EBP17_6.0 issued through Wisconsin Space Grant Consortium, and any opinions, findings, and conclusions or recommendations expressed in this material are those of the author(s) and do not necessarily reflect the views of the National Aeronautics and Space Administration.

References

Biba, K. (2009). High Altitude Wind Speed, Direction, and Air Temperature at Black Rock, Nevada for Amature Rocketry Application

Chang, M. C., Ray-Chaudhuri, T., Sun, L. L., & Wong, R. P. (1997). Acrylonitrile–Butadiene–Styrene (ABS) Polymers. In Handbook of Thermoplastics (pp. 135-159). New York, Basel, Hong Kong: Marcel Dekker, Inc.

Kulich, D. M., Gaggar, S. K., Lowry, V. and Stepien, R. (2003). Acrylonitrile–Butadiene–Styrene (ABS) Polymers. Kirk-Othmer Encyclopedia of Chemical Technology.

Kulich, D. M., Gaggar, S. K., Lowry, V. and Stepien, R. (2001). Acrylonitrile–Butadiene–Styrene Polymers. Encyclopedia of Polymer Science and Technology. 1.

Landau, L. D., & Lifshitz, E. M. (1970). The Theory Of Elasticity

Macmillan, H. A., Williams, C. M., Staples, J. F., & Sinclair, B. J. (2012). Reestablishment of ion homeostasis during chill-coma recovery in the cricket Gryllus pennsylvanicus. *Proceedings of the National Academy of Sciences,109*(50), 20750-20755. doi:10.1073/pnas.1212788109

Nomesh, K., & Venkateswara, R. V. (n.d.). Hyperelastic Mooney-Rivlin Model: Determination and Physical Interpretation of Material Constants. MIT Publications. doi:http://www.mitpublications.org/yellow_images/75618-me-book.43-46.pdf

Osborne, W. A. (n.d.). The Elasticity of Rubber Balloons and Hollow Viscera.doi:https://ia600701.us.archive.org/35/items/philtrans06128149/06128149.pdf